Jurnal Kejuruteraan 38(5) 2026: 2559-2570
https://doi.org/10.17576/jkukm-2026-38(5)-35

Study on the Effect of Secondary Pouring Interval on Tensile and Flexural Strength of Concrete with Cold Joints

Jun Wang[a,b], Kai Li[b*], Yamei Kong[a], Binhui Deng[b,c], Wenhui Qiu[d] & Jingyun Liu[a,b]

[a]*Henan Provincial Engineering Technology Research Center for Ecological High-Quality Utilization of Construction Solid Waste, Xuchang, Henan 461000,*

[b]*School of Civil Engineering, Xuchang University, Xuchang, Henan 461000,*

[c]*School of Civil Engineering and Transportation, North China University of Water Resources and Electric Power, Zhengzhou, Henan 450045,*

[d]*Henan Jinnuo Concrete Co., Ltd., Xuchang, Henan 461000.*

**Corresponding author: xculk@xcu.edu.cn*

Received 30 October 2025, Received in revised form 13 April 2026
Accepted 12 May 2026, Available online 30 August 2026

ABSTRACT

To enrich and refine the understanding of how secondary pouring intervals affect the mechanical properties of concrete with cold joints, building upon prior experimental studies examining the impact of cold joints on the mechanical properties of highly fluid C45 concrete, Abaqus software was employed to conduct finite element analysis on the splitting tensile strength and flexural strength of concrete with cold joints at multiple factor levels of secondary pouring time intervals ranging from 0.5T to 15T (where T represents the initial setting time of concrete). The results were compared with experimental data, showing consistent trends between finite element and experimental values, with errors within 10%. This demonstrates the applicability of the finite element model for analyzing the tensile and flexural properties of concrete with cold joints. Applying this model to explore the impact of cold joints on concrete mechanical properties at secondary pour intervals of 7-70d revealed that the effect diminishes and gradually stabilizes after 7 days. Compared to monolithic pouring, when secondary pouring occurred at 7d, 28d, 42d, and 56d, the splitting tensile strength decreased by 57.2%, 60.7%, 61.3%, and 61.9%, respectively, with reduction rates of 57.2%, 3.5%, 0.6%, and 0.6%. The flexural strength decreased by 59.9%, 67.6%, 68%, and 68.2%, respectively, with reduction rates of 59.9%, 7.7%, 0.4%, and 0.2%. This indicates that when the secondary pouring interval exceeds 28 days, the time interval has an extremely negligible effect on the mechanical properties of concrete with cold joints.

Keywords: Secondary pouring interval; concrete cold joint; splitting tensile strength; flexural strength

INTRODUCTION

As people's awareness of environmental protection increases, during the strict haze control process, "supply interruptions" often occur during concrete pouring due to construction control or other reasons. If the interruption time exceeds the initial setting period of the poured concrete, a "cold joint" in the concrete will be formed. The cold joint surface is also a weak point in the concrete structure (Fu et al. 2024; Kaja & Goyal 2023; Sandanayake 2022). The bonding quality between new and old concrete is influenced by numerous complex factors (Fu et al. 2022; Illangakoon et al. 2019), among which the interval time between pours is one of the most critical determinants.Recent scientific investigations into staged concrete pouring have revealed that the mechanical performance and durability of concrete structures are heavily dictated by the interval time between successive pours.

While discontinuities in pouring invariably create an "interlayer weak surface" or cold joint, research indicates that the detrimental impact on mechanical properties does not increase indefinitely but rather follows a specific stabilization and, in some metrics, a recovery pattern (Rathi & Kolase 2013).

Specifically, evidence suggests that the structural impact of the construction joint on mechanical degradation can diminish over time as the hydration degree develops with curing. While early-age (e.g., 7-day) tests often show significant strength loss at joints, the reduction rates for split tensile strength have been observed to decrease at 28 and 56 days, suggesting that the development of hydration products at the interface can partially compensate for the initial bonding weakness (Chen et al. 2024). Additionally, fracture mechanics analysis reveals that once a pouring interval reaches a certain duration such as 8 hours for standard C30 mixes parameters including the critical equivalent crack length and the fractal dimension of the fracture surface tend to stabilize (Fu et al. 2022). This indicates that the structural penalty for further increasing the pouring interval becomes marginal once the joint has fully transitioned to a brittle cracking mode (Fu et al. 2022; Deng et al. 2022).

To enrich and refine the understanding of how this interval affects the mechanical properties of concrete with cold joints, building upon prior experimental research on the mechanical properties of high-flowability C45 concrete with cold joints, using Abaqus software, finite element analysis was conducted on the splitting tensile strength and flexural strength of high-flowability concrete with cold joints at seven intervals ranging from 0.5T to 15T (where T represents the initial setting time of concrete). The results were compared with experimental data, validating the applicability of this finite element model for analyzing the tensile and flexural properties of concrete with cold joints. Using this model, the variation patterns of splitting tensile strength and flexural strength in concrete with construction joints were further analyzed for secondary pouring intervals ranging from 7 to 70 days. The results show that after the secondary pouring interval exceeds 7 days, the mechanical properties gradually become consistent. And after more than 28 days, the impact of construction joints on the decline of concrete mechanical properties can be ignored. This conclusion provides valuable guidance for the widespread application of high-flowability concrete in engineering projects.

EXPERIMENTAL OVERVIEW AND FINITE ELEMENT MODEL

EXPERIMENTAL OVERVIEW

The mix design for high-flowability concrete using washed sand from conventional sources is shown in Table 1. The concrete preparation and testing took place at the Engineering Structure and Testing Laboratory in early July, with an average ambient temperature of 27 ℃ and an average humidity of 45% RH. A HJW-60 single-horizontal-shaft mixer was employed for the mixing procedure. The dry materials were mixed for 60s, then half of the water and admixture were added and mixed for 90s, followed by the addition of the remaining water and admixture for another 60s. The mixture was placed in molds coated with a release agent and vibrated on a vibrating table for approximately 30s until no obvious bubbles appeared. The test blocks were demolded and numbered 24h after casting and immediately placed in a standard curing room until reaching the testing age of 28 days.

The concrete initial setting time and slump tests were conducted in accordance with the Test Code for Hydraulic Concrete (SL/T 352-2020). In this study, 'high-flowability' concrete is defined as concrete with a slump value greater than 200 mm that can fill molds primarily via self-flow, evaluated according to the SL/T 352-2020. The concrete initial setting time was measured as T=5h with a slump of 230mm. Tests on the splitting tensile and flexural properties of concrete with cold joints were conducted strictly according to the Standard for Test Methods of Physical and Mechanical Properties of Concrete (GB/T 50081-2019). This standard specifically permits the use of 150mm×150mm×150mm specimens for splitting tensile testing and 100mm×100mm×400mm specimens for flexural testing. For each time interval factor level, 5 sets of 150mm×150mm×150mm splitting tensile specimens and 5 sets of 100mm×100mm×400mm flexural specimens were cast. The cold joint angle was vertical. Specimen fabrication is illustrated in Figure 1. The formwork was placed vertically in the center of the mold. Concrete was poured on one side, while the formwork was secured on the opposite side with wooden blocks. After the specified time interval, the formwork and wooden blocks were removed. To simulate actual construction conditions, the interface treatment was adjusted dynamically according to the matrix strength. At the 0.5T, 1T, and 1.5T time points, the old concrete had not yet formed a spatial network structure with sufficient strength and could not withstand the impact of a high-pressure water gun; therefore, a scraper was utilized to physically remove the surface cement paste film. For specimens from 3T to 15T, the matrix had already developed early strength, so a high-pressure water gun was deployed to wash the bonding surface to elevate macroscopic roughness. The bonded surface of the old concrete was roughened, coated with a 3mm-thick layer of cement slurry, and then the remaining half of the concrete was poured. For splitting tensile and flexural tests, loads were applied along the cold joint surface. The time intervals ranging from 0.5T to 15T were specifically selected to realistically represent the different stages of old concrete development in construction practice: the plastic stage before initial setting (0.5T), the initial setting boundary (1T), the final setting point (1.5T), and the early hardening and strength development stages (3T, 6T, 9T, and 15T). This discretization accurately captures the critical transition periods where cooperative hydration ceases and the bond strength between the new and old concrete deteriorates most rapidly. Test values for splitting tensile and flexural strengths of high-flowability concrete with cold joints at secondary pouring intervals of 0.5T-15T are shown in Figure 2. The reported values in Figure 2 represent the average results of these specimens.

(a) Split tensile specimen (b) Flexural specimen

FIGURE 1. Process of preparing specimens with cold joints

TABLE 1. Mix proportions for C45 high-flowability concrete (kg/m^3)

Cement	Mineral Powder	Fly Ash	Coarse Aggregate	Small Stone	Stone powder	Washed Sand	Surface Sand	Admixture	Water
320	50	40	800	185	20	641	176	8.6	168

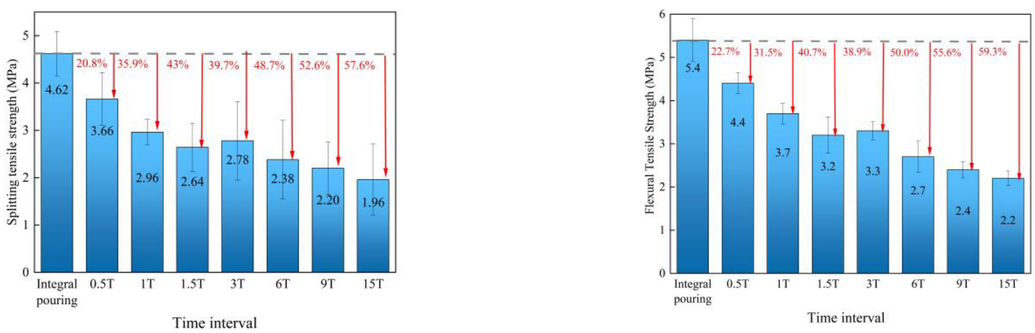

(a) Splitting tensile strength (b) Flexural tensile strength

FIGURE 2. Test values of tensile strength and flexural strength for concrete with cold joints.

FINITE ELEMENT MODEL

A finite element model was established using experimentally cast concrete specimens with cold joints as the research subject. The origin of the coordinate system was positioned at the geometric center of the specimen. Based on the three-zone bond model, finite element models were constructed for cubic splitting tensile and flexural specimens (Wu, 2012). These models simulated the effects of secondary pouring intervals on the splitting tensile and flexural properties of concrete with cold joints. Different secondary pouring intervals were represented by varying elastic moduli of the old concrete (Chen et al. 2008; Zheng, 2020).

COMPONENT CREATION

During modeling, the specimen is divided into three components: old concrete, cement paste interface layer, and new concrete. The interface layer thickness is set to 3 mm. Rigid pads are created to apply loads and boundary conditions: 20mm wide for splitting tensile tests and 5mm wide for flexural tests. The model was meshed using eight-node linear hexahedral elements (C3D8R). The splitting tensile test model comprised 8,400 elements, while the flexural test model contained 8,957 elements. The finite element model of the concrete specimen with a cold joint is shown in Figure 3.

MATERIAL PROPERTIES

The model contains four components: fresh concrete, old concrete, interface layer, and loading pad. Four distinct material properties must be defined and assigned to the corresponding components. The material property values for the interface layer and pad are shown in Table 2.

The material properties of concrete comprise density, elasticity (elastic modulus, Poisson's ratio), and plastic damage. The simulated concrete density is set to $2.4e^{-9}$ t/mm^3. According to the "Code for Design of Concrete Structures (GB50010-2024)" (Ministry of Housing and Urban-Rural Development of China, 2024), the Poisson's ratio for concrete ranges from 0.15 to 0.25, this study adopts a value of 0.2.

CONCRETE ELASTIC MODULUS

According to GB/T 50081-2019, standard concrete cubic specimens are tested after standard curing. Each specimen is centered in the compression machine, with a slight preload applied to ensure close contact between the specimen and platens. A continuous load at a rate of 0.5±0.1 MPa/s is steadily applied until failure. The maximum load is recorded, and compressive strength is calculated as the load divided by the bearing area, with the average of three valid specimens taken as the result. The measured cube compressive strengths of the highly fluid concrete at 3d, 7d, 14d, and 28d are shown in Table 3.

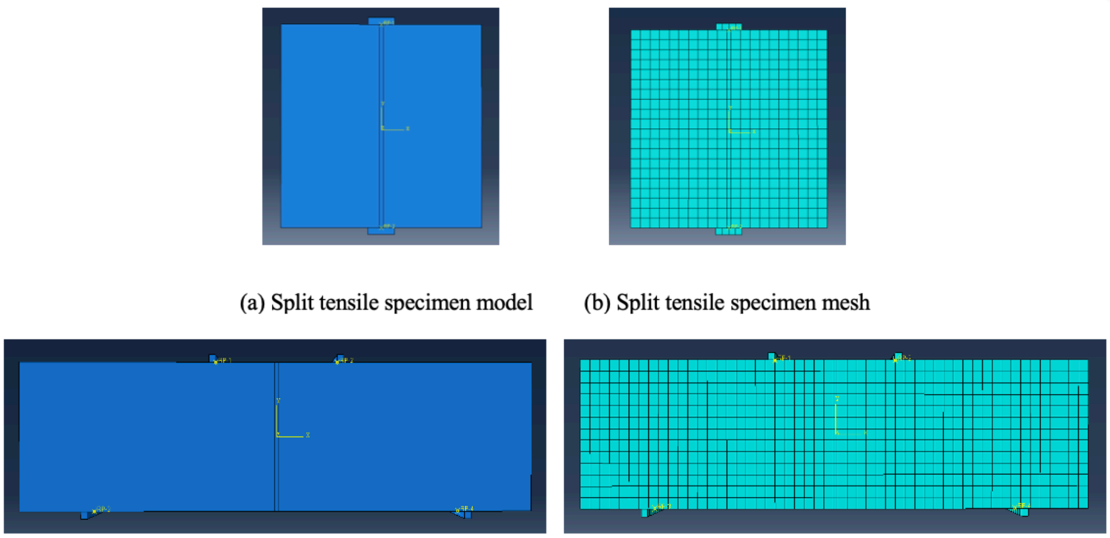

(a) Split tensile specimen model (b) Split tensile specimen mesh

(c) Flexural specimen model (d) Flexural specimen mesh

FIGURE 3. Finite element model of concrete with construction joints

Referencing the relationship between concrete strength and age, the cube compressive strength of monolithic cast specimens of high-flow concrete at arbitrary time intervals was estimated and corrected. The elastic modulus values of high-flow concrete at different time intervals were calculated using the formula $E_0 = \frac{100000}{2.2 + \frac{34.7}{f_{cu}}}$ (MPa) according to reference (Ministry of Housing and Urban-Rural Development of China, 2024), as shown in Table 4. The elastic modulus of fresh concrete was taken as 35853 MPa. For old concrete, except for the elastic modulus varying with the secondary pouring interval, all other parameters are consistent with those of new concrete.

TABLE 2. Material properties of interface layer and pad.

Material	Density (t/mm^3)	Modulus of Elasticity (MPa)	Poisson's Ratio
Interface Layer	3.1e^{-9}	30000	0.3
Spacer	7.85e^{-9}	210000	0.3

TABLE 3. Compressive strength of high-flowability concrete cubes at different ages (MPa).

Age	3d	7d	14d	28d
Compressive Strength/MPa	31.6	37.6	51.8	58.9

TABLE 4. Elastic modulus values for old concrete (MPa).

Time Interval	Integral Pour	0.5T	1T	1.5T	3T	6T	9T	15T
Age(d)	28	28.1	28.21	28.313	28.625	29.25	29.875	31.125
Compressive Strength (MPa)	58.9	58.94	58.99	59.03	59.17	59.45	59.73	60.26
Modulus of elasticity (MPa)	35853	35859	35865	35870	35888	35924	35959	36025

CONCRETE CONSTITUTIVE

The plastic damage model better describes the damage phenomena accompanying plastic deformation in concrete (Grassl & Jirásek 2006; Sarikaya & Erkmen 2019; Taqieddin & Voyiadjis 2009; Voyiadjis & Taqieddin, 2009). Based on the parameter identification method for the plastic damage model in references (Liu et al. 2020; Rakić et al. 2021; Sümer & Aktaş 2015), values for the plastic damage model are shown in Table 5. The parameter values for compressive and tensile behavior in the concrete plastic damage model are based on the concrete constitutive relationship in the GB50010-2024, as shown in Table 6.

INTERACTION BETWEEN NEW AND OLD CONCRETE

The interface layer between new and old concrete adopts selective surface contact, designating the concrete surface as the primary surface and the cement paste layer as the secondary surface. The slip formula employs minimal slip, permitting very slight relative movement between the two contact surfaces. Contact properties are set as friction and cohesion contact, with surface-based cohesive behavior and friction contact defined concurrently in Abaqus Interaction Module. The friction model selects "penalty" for tangential behavior, while the normal behavior defaults to "hard contact". The cohesion model primarily involves three parameters: stiffness, strength, and fracture energy. This study assumes that normal stiffness and tangential stiffness remain constant across different roughness levels. The normal stiffness is set to 3500 MPa, tangential stiffness to 1500 MPa, and fracture energy to 100 J/m² (Hu et al. 2021; Wittmann et al. 2010). The damage initiation criterion employs the maximum stress criterion.

Strength includes three components: normal contact stress t_n, shear contact stress t_s in the first shear direction, and shear contact stress t_t in the second shear direction. t_s and t_t are set to 2 MPa (Chen et al. 2014). Based on the normal critical stress at the interface, typically ranging from 68.6% to 84.2% of the strength ratio between new and old concrete. Taking the critical stress along the interface t_n=0.75f_t,f_t=0.24 $f_{cu}^{2/3}$, where f_t is the axial tensile strength of the concrete specimen and f_{cu} is the cube compressive strength of the concrete specimen with a cold joint, substituting yields t_n. Specific values are shown in Table 7.

VERIFICATION OF FINITE ELEMENT MODEL APPLICABILITY

SPLITTING TENSILE STRENGTH

Through finite element simulation analysis, the stress distribution during deformation and the crack propagation process after failure can be observed in specimens with cold joints. Figure 4 shows the stress contour map when the concrete specimen with a cold joint reaches its ultimate load during the splitting tensile test. As seen in Figure 4, tensile stresses near the cold joint bond surface exceed those in the new and old concrete sections, indicating that the cold joint region is a potential failure or rupture location and represents the weak link in the composite specimen. Stress concentration occurs at the interface between the cold joint bonding surface and the spacer block. This is because during simulated splitting tensile tests, the applied load is concentrated at the upper and lower edges of the cold joint. Consequently, specimen failure consistently initiates at the loading end, with stress propagating inward along the cold joint surface. When the load reaches the critical value, the crack propagation path closely aligns with that observed during testing.

Experimental and analytical values for splitting tensile tests of concrete with cold joints under different secondary pouring intervals are shown in Table 8. As indicated in Table 8, analytical values for splitting tensile strength closely match experimental results, generally exceeding them. This discrepancy primarily stems from the uniform loading rate maintained during testing, whereas Abaqus employs displacement-controlled loading. Displacement control allows stresses in the concrete crack propagation zone to fully release, resulting in higher measured peak loads. However, the error remains within 11%, and both analytical and experimental values exhibit identical trends in splitting tensile strength. This confirms the validity of the finite element model for splitting tensile testing.

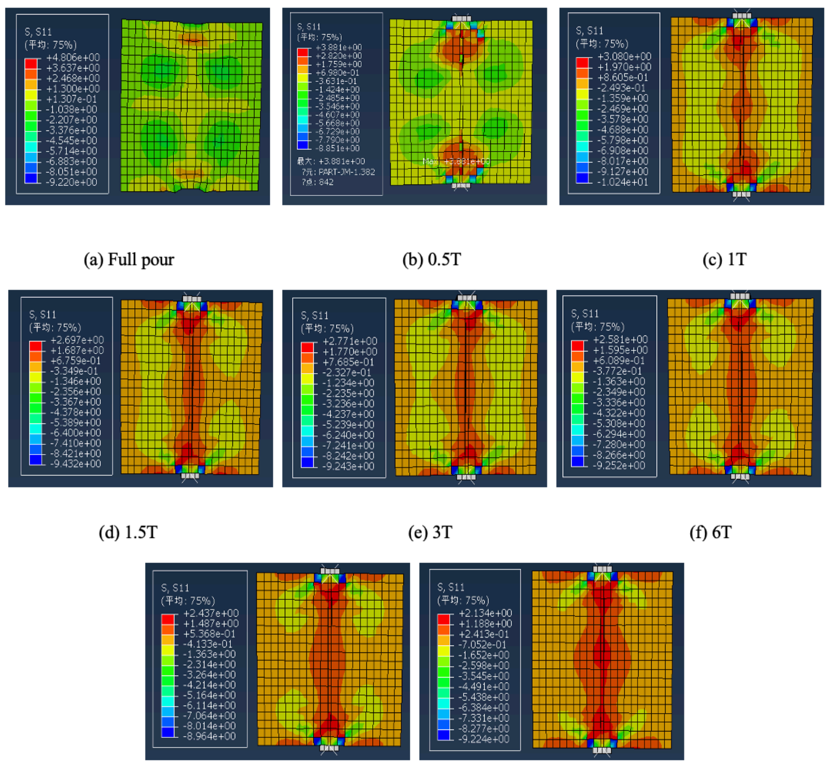

(a) Full pour (b) 0.5T (c) 1T

(d) 1.5T (e) 3T (f) 6T

(g) 9T (h) 15T

FIGURE 4. Strss contour map of splitting tensile model.

TABLE 5. Parameters of the plastic damage model for concrete.

Expansion angle	Eccentricity	f_{b0} / f_{c0}	K	Viscous parameter
30°	0.1	1.16	0.667	0.001

TABLE 6. Control parameters for concrete plastic damage models (MPa).

f_{cu}	E_c	f_c	f_t	f_{ce}	$\boldsymbol{k}_c$	$\boldsymbol{K}_t$
59.1	35879.1	39.6	3.0	15.8	0.7	0.5

TABLE 7. Strength values in cohesive models (MPa).

Time Interval	0.5T	1T	1.5T	3T	6T	9T	15T
f_{cu}	52.9	49.3	45.6	45	41.2	39.6	37.1
t_n	2.54	2.41	2.3	2.28	2.15	2.09	2

TABLE 8. Comparison of splitting tensile strength results.

Time Interval	Continuous Pour	0.5T	1T	1.5T	3T	6T	9T	15T
Test Value (MPa)	4.62	3.66	2.96	2.64	2.78	2.38	2.20	1.96
Analyzed Value (MPa)	4.81	3.88	3.08	2.70	2.77	2.58	2.44	2.13
Difference (MPa)	0.19	0.22	0.12	0.06	0.01	0.2	0.24	0.17
Percentage Error	4.1%	6%	4%	2.3%	0.3%	8.4%	10.9%	8.7%

FLEXURAL STRENGTH

Figure 5 shows the stress distribution map of the simulated flexural test specimen with a cold joint reaching ultimate bearing capacity. The stress distribution map of the monolithic concrete specimen indicates that under a bending moment, the stress is highest in the pure bending region at the midspan of the bottom of the concrete specimen, gradually decreasing toward both ends. The vertical cold joint occupies the region of maximum tensile stress. The stress distribution map of the cold-jointed concrete specimen reveals that tensile stresses on both sides of the cold joint are significantly higher than those in the main body of the new and old concrete. As the applied load increases, cracks first appear at the cold joint surface on the bottom of the specimen. Simultaneously, the maximum stress migrates upward along the cold joint surface, causing the crack to propagate. When the load reaches a certain value, the crack penetrates the cold joint surface, leading to specimen failure. The failure path in the finite element simulation is essentially consistent with that observed in the experimental failure.

Considering the stress contour plots from both the splitting tensile and flexural models, due to differences in elastic modulus between fresh and aged concrete resulting from varying curing periods, the stress distributions on the left and right sides of the specimen exhibit asymmetry during loading. In Abaqus simulations, cracking initiates from the outer edge of the element, leading to two scenarios depicted in Figure 5: cracking originating from the fresh concrete side and cracking originating from the aged concrete side. In actual testing, multiple failure locations were observed. For instance, when the secondary pouring interval was short (e.g., 0.5T, 1T), the cement slurry bonding agent exhibited superior adhesion, resulting in strong interface integrity with the concrete. This manifested as failure occurring solely within the concrete matrix. As the interval between pours increases (e.g., 1.5T, 3T, 6T), the bonding effectiveness of the interface agent diminishes. Cracks developing within the concrete gradually migrate toward the interface layer, ultimately propagating along it. This results in the simultaneous failure of both the concrete and the interface layer. When the secondary pouring interval is extended to 9T or 15T, specimens exhibit failure only at the bonding interface between the primer and the later-poured concrete, with the concrete on both sides remaining intact.

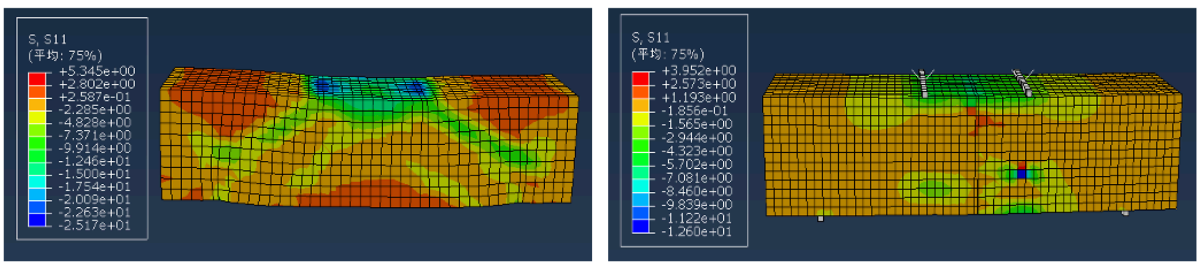

(a) Continuous Pour (b) 0.5T

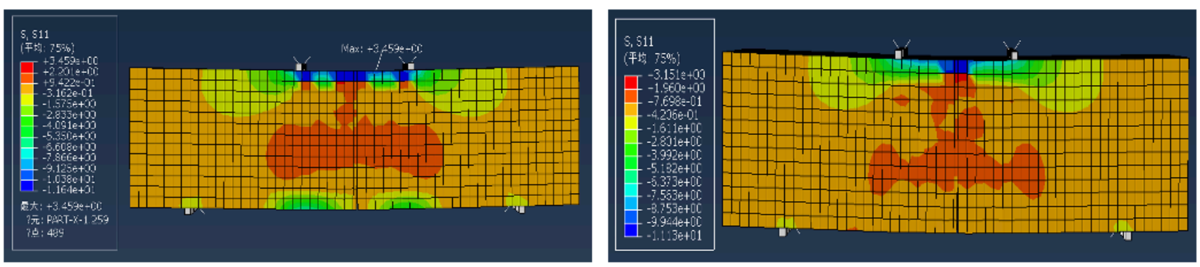

(c) 1T (d) 1.5T

continue...

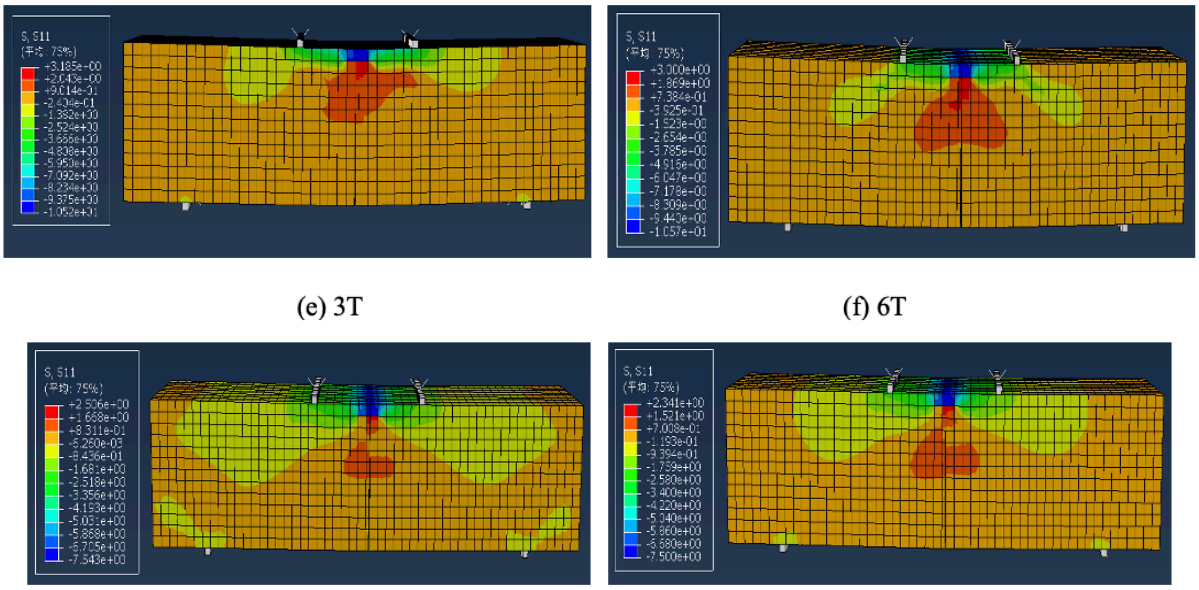

(e) 3T (f) 6T

(g) 9T (h) 15T

FIGURE 5. Stress cloud diagram of flexural model.

Test values and finite element analysis values for flexural strength specimens with cold joints under different secondary pouring intervals are shown in Table 9. As indicated in Table 9, the analyzed flexural strength values closely match the test values, with errors generally maintained within 11%. Furthermore, both analyzed and test values exhibit similar trend patterns, confirming the feasibility of the flexural strength model used in finite element simulations.

TABLE 9. Comparison of flexural strength values.

Time Interval	Integral Pour	0.5T	1T	1.5T	3T	6T	9T	15T
Test Value (MPa)	5.36	4.36	3.66	3.16	3.28	2.72	2.36	2.16
Analyzed Value (MPa)	5.34	3.95	3.46	3.15	3.19	3.00	2.51	2.34
Difference (MPa)	-0.02	-0.41	-0.2	0.01	-0.09	0.28	0.15	0.18
Percentage Error	0.4%	9.4%	5.5%	0.3%	2.7%	10.3%	6.4%	8.3%

MECHANICAL PROPERTIES OF CONCRETE WITH COLD JOINTS UNDER EXTENDED SECONDARY POURING INTERVALS

SPLITTING TENSILE STRENGTH

Stress contour plots of the splitting tensile model for concrete with cold joints under different secondary pouring intervals are shown in Figure 6. Figure 6 indicates that the stress distribution patterns during splitting failure of specimens at 7d to 70d are similar to those at 15T (T=5h). This suggests that when the secondary pouring interval exceeds 3d, although the splitting tensile strength of cold-jointed concrete specimens exhibits some fluctuation, the failure mechanisms and stress transfer pathways remain fundamentally consistent.

The analytical values for the tensile strength of concrete with cold joints under different secondary pouring intervals are shown in Table 10. As shown in Table 10, the variation in splitting tensile strength of concrete with cold joints diminishes as the secondary pouring interval increases. The splitting tensile strength values at 14d and 28d intervals differ by only 0.1 MPa, with a strength reduction rate of just 2.1% compared to monolithic specimens. This aligns with existing experimental conclusions from Fu et al. (2022) and Deng et al. (2023). Compared to monolithic specimens, the reduction rates in splitting tensile strength at 7d, 28d, 42d, 56d, and 70d were 57.2%, 60.7%, 61.3%, 61.9%, and 62.1%, respectively. The cumulative decrease across these intervals was 57.2%, 3.5%, 0.6%, 0.6%, and 0.2%, respectively. This indicates that after a 7-day interval, the impact of cold joints on splitting tensile strength diminishes, and beyond 28 days, extended intervals have a negligible effect on splitting tensile performance.

FLEXURAL STRENGTH

Figure 7 shows the stress distribution map of the flexural model for concrete with cold joints under extended secondary pouring intervals. As depicted in Figure 7, stress transfer accelerates during flexural testing of specimens after 14 days, leading to a relatively rapid failure process. While flexural strength exhibits some fluctuation in specimens with cold joints, stress consistently propagates upward along the cold joint surface, ultimately causing cracking along this interface.

Analytical values for flexural strength of concrete with cold joints under different secondary pouring intervals are shown in Table 11. As shown in Table 11, the flexural strength of concrete with cold joints gradually decreases with increasing secondary pouring intervals, though the rate of decrease becomes progressively smaller. Compared to monolithic specimens, the flexural strength reduction rates at intervals of 7d, 28d, 42d, 56d, and 70d were 59.9%, 67.6%, 68%, 68.2%, and 68.4%, respectively. with respective decreases of 59.9%, 7.7%, 0.4%, 0.2%, and 0.2%. This indicates that, after 7 days, the effect of the secondary pouring interval on the flexural strength of cold-joint concrete gradually diminishes and stabilizes. After 28 days, an increase in the interval time has virtually no effect on the decline in the concrete's flexural performance.

TABLE 10. Analysis values of split tensile strength for concrete with cold joints under different secondary pouring intervals.

Time Interval	Integral Pour	7 d	14 d	21d	28d	42 d	56 d	70 d
Analysis Value (MPa)	4.81	2.06	1.99	1.95	1.89	1.86	1.83	1.82
Decrease (MPa)	--	2.75	2.82	2.86	2.92	2.95	2.98	2.99
Percentage Decrease	--	57.2%	58.6%	59.5%	60.7%	61.3%	61.9%	62.1%
Decrease Amplitude	--	--	1.4%	0.9%	1.2%	0.6%	0.6%	0.2%

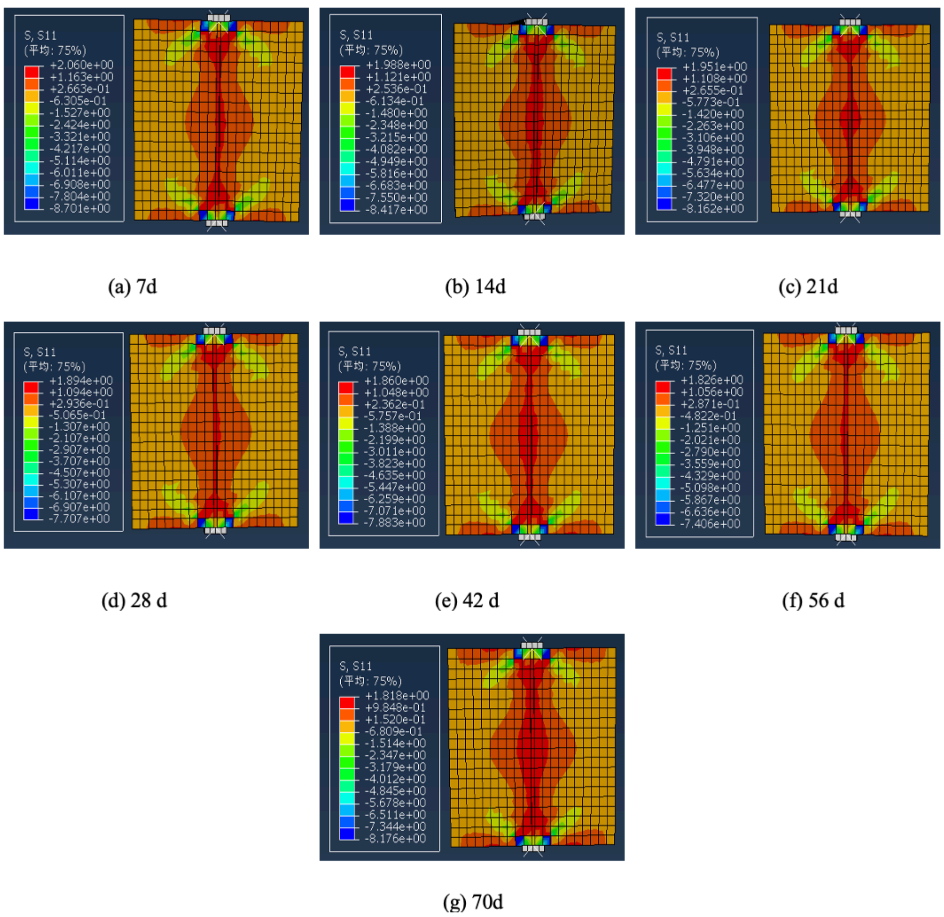

FIGURE 6. Stress contour map of concrete split-tensile model with cold joint under different secondary pouring intervals

Figure 8 shows the time-dependent variation curves of the analytical values for the splitting tensile strength and flexural strength of concrete with cold joints as a function of the secondary pouring interval. As shown in Figure 8, both curves exhibit consistent trends that gradually flatten. This indicates that although the strength of concrete with cold joints continues to decrease with increasing secondary pouring interval, the rate of decline diminishes progressively and stabilizes. It should also be noted that the extent of the decrease varies across different time intervals; for example, the reduction in splitting tensile strength and flexural strength at 9T and 15T. Although both splitting tensile failure and flexural failure are governed by tensile stress, differences in stress distribution under varying loading conditions can lead to a reversal of this sensitivity. In bending tests, the bending moment generates a local maximum tensile stress at the bottom fibers at the mid-span position, thereby directly applying stress to the discontinuities on the surface of the cold joint. In contrast, the splitting tensile test creates a more uniform tensile stress field at the center plane. Consequently, flexural strength is more sensitive to surface defects and differential shrinkage during the early hardening stage (9T), whereas the internal bond strength does not completely fail in resisting splitting tensile failure until a later stage (15T). What's more after the secondary pouring interval exceeds 28 days, further increases in the interval have a negligible effect on the splitting tensile and flexural properties of concrete with cold joints.

TABLE 11. Analysis of flexural strength values for concrete with cold joints under different second pouring intervals

Interval	Integral Pour	7d	14d	21d	28d	42 d	56 d	70 d
Analysis Value (MPa)	5.34	2.14	1.99	1.87	1.73	1.71	1.70	1.69
Decrease (MPa)		3.2	3.35	3.47	3.61	3.63	3.64	3.65
Percentage Decrease		59.9%	62.7%	65%	67.6%	68%	68.2%	68.4%
Decrease Amplitude			2.8%	2.3%	2.6%	0.4%	0.2%	0.2%

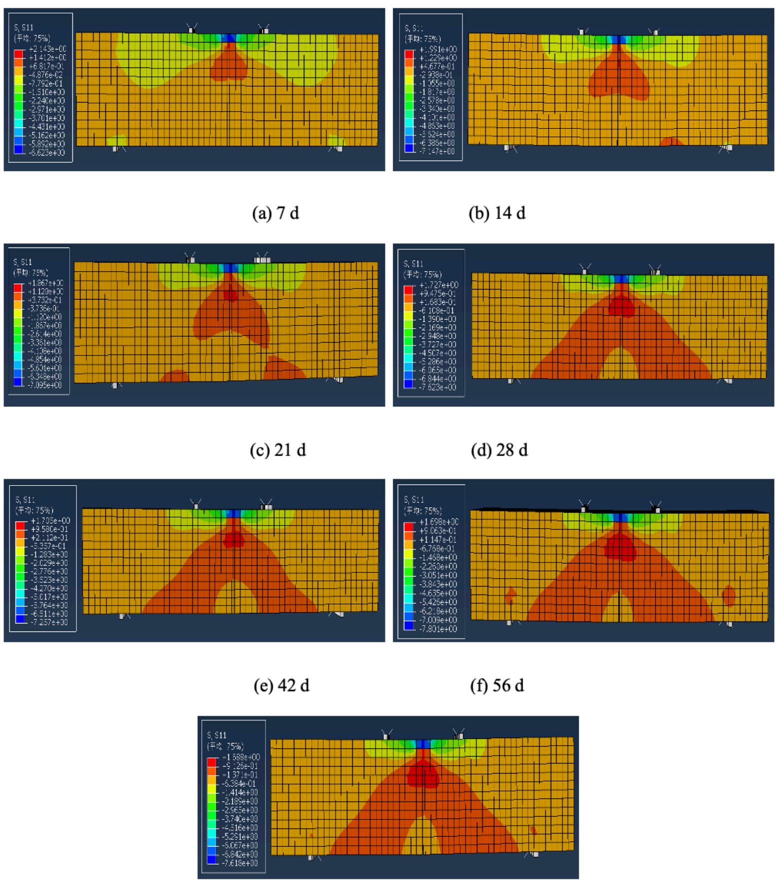

(a) 7 d (b) 14 d

(c) 21 d (d) 28 d

(e) 42 d (f) 56 d

(g) 70d

FIGURE 7. Stress contour map of flexural strength model for concrete with cold joints under different secondary pouring intervals

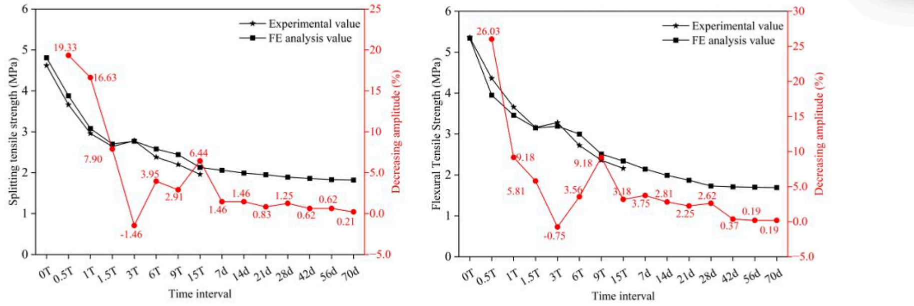

(a) Splitting tensile strength (b) Flexural tensile strength

FIGURE 8. Strength variation curve of concrete with cold joints under the influence of time interval

CONCLUSIONS

1. Short secondary pouring intervals significantly degrade the mechanical properties of concrete, especially when the interval occurs before the final setting time (1.5T). The adverse effect of construction cold joints is much more pronounced on tensile and flexural strengths than on compressive strength.
2. Flexural strength exhibits an earlier sensitivity to the cold joints compared to splitting tensile strength. Complete interface failure is observed at 9T for flexural tests, but at 15T for splitting tensile tests, reflecting the heightened sensitivity of flexural loading to localized extreme tensile stresses at the joint discontinuity.
3. The finite element model established using Abaqus successfully simulated the failure patterns and mechanical properties, with analysis values deviating from test values by less than 10%, proving its applicability for analyzing jointed structures.
4. Extended time interval analyses indicate that the impact of construction joints on the strength reduction gradually stabilizes after 7 days. Beyond a 28-day interval, increasing the pouring delay has a negligible further effect on the overall tensile and flexural mechanical properties of the structure.
5. In engineering practice, if a cold joint is unavoidable, the secondary pouring should be completed as early as possible before the final setting to minimize structural weakness.

DATA AVAILABILITY STATEMENT

The data that support the findings of this study are available on request from the corresponding author. The data is not publicly available due to privacy or ethical restrictions.

ACKNOWLEDGEMENT

The authors would like to acknowledge financial support from the National Natural Science Foundation of China under Grant No.12402075, Henan Provincial Science and Technology Research Project under Grant No.252102321178, Youth Project of Natural Science Foundation of Henan Province under Grant No. 252300423446 and Key Scientific Research Project of Institutions of Higher Education in Henan Province under Grant No.26B560019.

DECLARATION OF COMPETING INTEREST

None.

REFERENCES

Chen, F., Zheng, J. L., Yu, B. L. 2008. Finite element simulation of the shrinkage performance of adherence between self-compacting concrete and old concrete. *Journal of Huazhong University of Science and Technology (Urban Science Edition)* 25(4): 219-222.

Chen, F. F., Wu, Y. X. 2014. The coupling analysis of fracture and contact fornew-to-old concrete interface. *Low-Temperature Construction Technology* 2014(1): 108-111.

Chen, Z., Huang, Z., Wei, J., Zhao, G., & Tang, Y. 2024. The mechanical properties and chlorine resistance of concrete based on the effects of pouring interval time. *Buildings* 14(6): 1558.

Deng, H. S., Fu, H. L., Li, H., Shi, Y., & Huang, Z. 2023. Fracture performance and fracture characteristics of concrete members with cold joints: Numerical simulation. *Theoretical and Applied Fracture Mechanics* 125: 103868.

Deng, H. S., Fu, H. L., Zhao, Y. B., Shi, Y., & Huang, X. 2022. Using acoustic emission parameters to study damage and fracture characteristics of concrete with different pour intervals cold joints. *Theoretical and Applied Fracture Mechanics* 122: 103601.

Fu, H. L., Deng, H. S., Shi, Y., Wu, Y. M., & Zhao, Y. B. 2024. Analysis method for cracking and safety status of plain concrete lining with cold joints. *Case Studies in Construction Materials* 21: e03696.

Fu, H. L., Deng, H. S., Zhang, J., Shi, Y., & Huang, X. 2022. Experimental analysis of influence of pouring interval on fracture performance of concrete structures with cold joints. *Theoretical and Applied Fracture Mechanics* 118: 103289.

Grassl, P., & Jirásek, M. 2006. Damage-plastic model for concrete failure. *International Journal of Solids and Structures* 43(22-23): 7166-7196.

Hu, B., Meng, T. F., Li, Y., Li, D. Z., & Chen, L. 2021. Dynamic splitting tensile bond behavior of new-to-old concrete interfaces. *Construction and Building Materials* 281: 122570.

Illangakoon, G. B., Asamoto, S., Nanayakkara, A., & Trong, L. N. 2019. Concrete cold joint formation in hot weather conditions. *Construction and Building Materials* 209: 406-415.

Kaja, N., & Goyal, S. 2023. Impact of construction activities on environment. *Resource*, 45: 50.

Liu, Q. F., Guo, W., & Kuang, Y. H. 2020. Parameter calculation and verification of concrete plastic damage model of ABAQUS. *IOP Conference Series: Materials Science and Engineering* 794(1): 012036.

Ministry of Housing and Urban-Rural Development of China. 2024. Code for Design of Concrete Structures: GB50010-2024. Beijing: China Architecture & Building Press.

Ministry of Housing and Urban-Rural Development of the People's Republic of China, State Administration for Market Regulation. 2019. Standard for Test Methods of Physical and Mechanical Properties of Concrete: GB/T 50081-2019. Beijing: China Architecture and Building Press.

Ministry of Water Resources of the People's Republic of China. 2020. Test Code for Hydraulic Concrete: SL/T 352-2020. Beijing: China Water Power Press.

Rakić, D. M., Bodić, A. S., Milivojević, N. J., Dunić, V. L., & Živković, M. M. 2021. Concrete damage plasticity material model parameters identification. *Journal of the Serbian Society for Computational Mechanics* 15(2): 111-122.

Rathi, V. R., & Kolase, P. K. 2013. Effect of cold joint on strength of concrete. international journal of innovative research in science, *Engineering and Technology* 2(9): 4671-4678.

Sandanayake, M. S. 2022. Environmental impacts of construction in building industry-A review of knowledge advances, gaps and future directions. *Knowledge* 2(1): 139-156.

Sarikaya, A., & Erkmen, R. E. 2019. A plastic-damage model for concrete under compression. *International Journal of Mechanical Sciences* 150: 584-593.

Sümer, Y., & Aktaş, M. 2015. Defining parameters for concrete damage plasticity model. *Challenge Journal of Structural Mechanics* 1(3): 149-155.

Taqieddin, Z. N., & Voyiadjis, G. Z. 2009. Elastic plastic and damage model for concrete materials: Part II: Implementation and application to concrete and reinforced concrete. *International Journal of Solids and Structures-Mechanics and Applications* 1(1): 187-209.

Voyiadjis, G. Z., & Taqieddin, Z. N. 2009. Elastic plastic and damage model for concrete materials: Part I-theoretical formulation. *International Journal of Solids and Structures-Mechanics and Applications* 1(1): 31-59.

Wittmann, F. H., Sun, Z., & Zhao, T. 2010. Surface energy and fracture energy. *Proceedings of the 7th International Conference On Fracture Mechanics Of Concrete And Concrete Structures* 13-18.

Wu, K. Z. (2012). Research and Finite Element Analysis on Bonding Performance of New and Old Concrete. Master's Thesis, Xihua University.

Zheng, G. F. (2020). The Effect of HEC Interface Agent on the Bond Strength of the Third Age RCC. Master's Thesis, Xi'an University of Technology.